Virtual Impedance Control for Load Sharing and Bus Voltage Quality Improvement in Low Voltage AC Microgrid

Xiao, J.; Wang, L.; Bauer, P.; Qin, Z.

DOI
10.1109/TSG.2023.3325620

Publication date
2023

Document Version
Final published version

Published in
IEEE Transactions on Smart Grid

Virtual Impedance Control for Load Sharing and Bus Voltage Quality Improvement in Low-Voltage AC Microgrid

Junjie Xiao, *Graduate Student Member, IEEE*, Lu Wang, *Graduate Student Member, IEEE*, Pavol Bauer, *Senior Member, IEEE*, and Zian Qin, *Senior Member, IEEE*

***Abstract*—Due to the mismatched feeder impedances in a resistive feeder AC microgrid, it's challenging to accurately share harmonic and active power while promising a low bus voltage distortion rate. To address this issue, this paper proposes a distributed philosophy-based virtual impedance modulation strategy. The proposed method regulates the fundamental and harmonic impedance at the desired value by exchanging information with its adjacent inverters. Notably, the proposed method benefits from resilience against communication delay, failure, and cyber-attacks. Moreover, it significantly reduces the communication burden. The proposed method's effectiveness is validated through experiments conducted in various cases, including different communication scenarios and plug-and-play operations.**

***Index Terms*—AC microgrid, adaptive virtual impedance, power sharing, distributed control.**

I. Introduction

MICROGRID is a small-scale power system composed of multiple distributed generation (DG) units. It is an attractive field [1] as it provides a promising solution for substantial economic and environmental benefits.

In a low-voltage microgrid, the droop law (Q-ω, P-V) is widely used to regulate power flow [2], as the feeders feature in resistor property [3]. Although the frequency is a global variable and reactive power can be proportionally shared [4], achieving active power sharing remains challenging due to mismatched line impedance. Moreover, in microgrid systems, the proliferation of sensitive loads is primarily nonlinear [5], [6], necessitating proper sharing of the harmonic power generated by these loads among the units, which traditional droop law disregards. Various power-sharing strategies have been proposed to address these challenges, and they can be broadly classified into two categories: local state-based methods and communication-based methods [7].

The virtual impedance technique is effective in achieving accurate power-sharing. This technique modifies the voltage controller reference by incorporating an output current feed-forward loop, as studies such as [3] demonstrate. While it may seem intuitive to compensate for the impedance difference by measuring the real line impedance of each feeder, identifying the physical feeder impedance in practice is generally costly. Besides, some scholars propose adding a sizeable virtual impedance to the controller [8]. However, this approach can lead to significant distortion in the Point of Common Coupling (PCC) voltage.

The implementation of the control methods outlined in [9], [10] necessitates the utilization of a Microgrid Central Controller (MGCC), which regulates the virtual impedance based on real-time measurements and references of power. However, it is noteworthy that the dependence on the central controller renders the system susceptible to a single point of failure.

To address issues of communication failure, the microgrid system employs a distributed philosophy to improve scalability and reliability. In recent research presented in [11], [12], consensus-based distributed control was implemented in parallel inverter systems, with units propagating information to adjacent agents. However, limited communication resources can pose a significant challenge to the distributed philosophy employed in microgrid systems, resulting in suboptimal system performance [13]. Previous studies have proposed periodic data exchange with adjacent agents as a method of reducing communication burden [14], [15]. An alternative approach involves using a discrete-time communication mechanism to update neighbour states, which is promising in conserving communication resources [16]. The communication-based event-triggered control (ETC) approach has gained significant attention in the multi-agent system (MAS) field due to its ability to schedule communication networks intelligently. Thus, it is possible to reduce the communication burden compared to the typical approach [17].

Nevertheless, the enormous traffic pressure on the communication network in practical applications will not be alleviated as many loads on the AC bus continually switch [17]. Therefore, the communication burden of distributed control-based virtual impedance modulation remains challenging.

Manuscript received 17 March 2023; revised 20 June 2023 and 1 October 2023; accepted 8 October 2023. Date of publication 18 October 2023; date of current version 23 April 2024. This work was supported by the China Scholarship Council under Grant 202106280042. Paper no. TSG-00387-2023. *(Corresponding author: Zian Qin.)*

The authors are with the DC System, Energy Conversion and Storage Group, Faculty of Electrical Engineering, Mathematics and Computer Science, Delft University of Technology, 2628 CD Delft, The Netherlands (e-mail: J.Xiao-2@tudelft.nl; L.Wang-11@tudelft.nl; P.Bauer@tudelft.nl; z.qin-2@tudelft.nl).

Color versions of one or more figures in this article are available at https://doi.org/10.1109/TSG.2023.3325620.

Digital Object Identifier 10.1109/TSG.2023.3325620

Moreover, The communication-based method, while introducing communication technology, can benefit the accurate sharing of active and harmonic power, it is vulnerable to cyber attacks [11], which may adversely affect overall control accuracy and cause instability [18]. A common strategy to combat cyber attacks involves detecting the attack and implementing suppression measures. Cyber attack detection methods typically fall into two categories based on their reliance on models. The first category is model-based approaches, exemplified using Kalman filter-based detectors in [19]. While these methods can effectively identify FDIAs in power systems, they have a significant drawback: obtaining accurate physical models is challenging in real-world scenarios. This approach becomes less effective when challenged by smart attacks [20]. Conversely, model-free approaches, such as AI-based algorithms mentioned in [21], hold the promise of network attack detection but come with an increased computational burden [22].

The existing body of research on enhancing resilience against cyber-attacks primarily toward full resilience in microgrids [23], albeit at the cost of increased computational and communication burden. Another approach involves introducing adaptive feedback terms to counteract FDI signals [24], but this method results in a slower response speed for cyber attack mitigation. Additionally, reducing the weight of the attacker channel in communication is considered an effective approach [18], [25]; however, even with significant reductions, the effectiveness of the cyber attack still persists within the system.

Based on the above literature review, several significant research gaps can be identified as follows: (a) The existing research predominantly concentrates on medium-voltage AC microgrids. However, there is insufficient research on the application of virtual impedance in low-voltage AC microgrids. We highlight the distinct characteristics of these two systems, particularly the impact of droop control on the implementation of virtual impedance [8], [9], [10], [12], [26]. (b) Harmonic power-sharing may introduce a sizeable virtual impedance, leading to a degradation of the Point of Common Coupling (PCC) voltage quality, which is ignored in [9], [10], [12], [13]. (c) The communication burden remains a challenge in the distributed virtual impedance for power sharing. [13], [14], [15], [16], [17]. (d) The effectiveness of cyber attack detectors is diminished by inaccurate models and the associated computational burden [19], [20], [21], [22]. (e) Conventional resilience approaches for cyber attacks result in computational complexity and fail to completely eliminate the attack [18], [23], [24], [25]. (f) While there have been studies on multi-unit systems, we can hardly find any research investigating cyber attacks in the communication-based virtual impedance.

Motivated by the identified research gaps, this paper presents a distributed communication-based virtual impedance control method that addresses the challenges of achieving resilience and low communication burden while enabling active power, harmonic power sharing, and PCC voltage compensation in low-voltage AC microgrids. The comparison of the proposed approach with the counterparts can be illustrated in Fig. 1, and the contributions of this paper are outlined as follows:

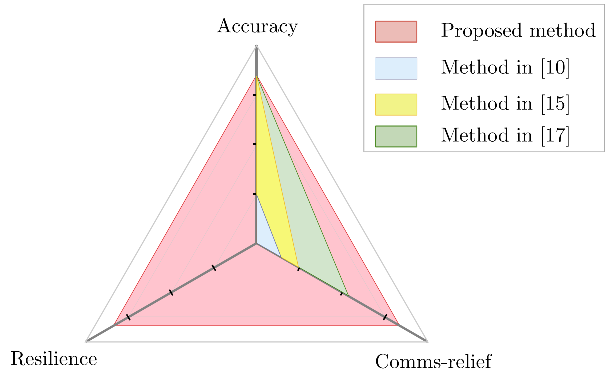

Fig. 1. The comparison of the proposed and other representative studies.

(1) This study introduces a novel consideration of voltage quality, encompassing fundamental and harmonic power in low-voltage AC microgrids. By avoiding the sizeable harmonic virtual impedance, the proposed method enhances PCC voltage quality.

(2) The proposed method significantly alleviates the communication burden by eliminating the need for communication networks once the virtual impedance has been adjusted.

(3) This paper is pioneering research on the implications of cyber attacks on distributed virtual impedance. Moreover, The proposed approach doesn't rely on cyber attack detection and thus responds swiftly to attack signals.

(4) The proposed cyber attack mitigation algorithm offers computational savings compared to full resilience towards methods by leveraging a reasonable assumption that the hacker cannot compromise the entire communication network due to the diverse characteristics of the communication measures within the microgrid system.

(5) This study pioneers research on cyber attack mitigation in the context of communication-based virtual impedance. A practical method is proposed that disregards compromised communication channels, thereby improving the response speed to attack mechanisms and effectively eliminating attack signals.

(6) The proposed virtual impedance strategy adopts a distributed approach, eliminating the risk of single points of failure, and its stability is validated using Lyapunov criteria. The adaptability of the control strategy is also assessed under conditions such as communication failures and cyber-attacks.

The paper is organized as follows: Section II explains the investigated inverter system's operation principle. Section III presents the proposed communication-based virtual impedance for power sharing and harmonic voltage compensation methods. The FDIA model and resilient controller are presented in Section IV, along with the communication relief controller and Lyapunov theory-based stability analysis. Section V provides extensive experimental results demonstrating the proposed control strategy's effectiveness. Finally, the article is concluded in Section VI.

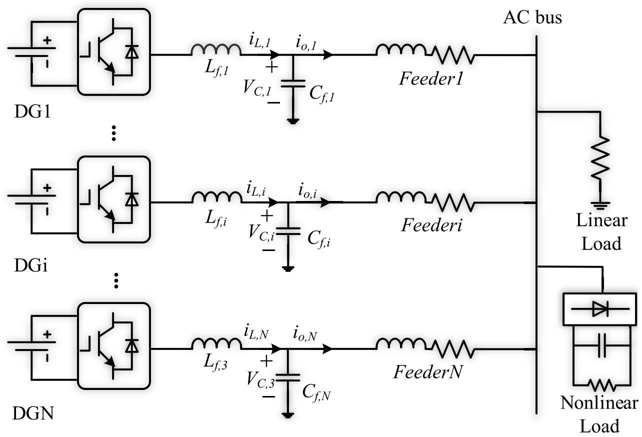

Fig. 2. The scheme of a microgrid with N inverters.

II. Island Microgrid Control

Fig. 2 depicts a schematic of island microgrids that incorporates a variety of loads, including linear and nonlinear loads. The participating agents are connected to the AC bus through an LC filter and feeder. The parameters of the adopted filter, namely the inductor and capacitor, are denoted by L_f and C_f, respectively. The feeder takes on resistor characteristics. The current of the filter inductor is represented by $i_{L,i}$, while the voltage of the capacitor is represented by $V_{C,i}$. Additionally, the output current of DGi is denoted by $i_{o,i}$.

A. Primary Control

The *P*-*V* and *Q*-*ω* droop laws are extensively utilized in resistive feeder systems for power flow regulation, as demonstrated in equations (1) and (2):

$$\omega_i = \omega^* + n_{qi} Q_i \tag{1}$$

$$V_i = V^* - m_{pi} P_i \tag{2}$$

where ω_i and V_i represent the frequency and voltage amplitude; ω^* and V^* are the nominal set points of frequency and voltage amplitude; P_i and Q_i are the calculated active power and reactive power of *ith DG*; The droop coefficient m_{pi} and n_{qi} should be set as inverse as the maximum power rating of *DGs*. As ω_i in (1) is the global variable, which means the output frequency among the participating converters is the same, the active power could be proportionally shared, $n_{Q1}Q_1 = n_{Q2}Q_2 = \cdots = n_{qi}Q_i$. However, it is challenging to reach active power sharing because of the mismatched feeder impedance, which will be detailed in Section II-B.

The reference for the inner controller that manages the actual output voltage of the filter capacitor is derived from the outcome of the droop control. It can be written as (3):

$$V_{d,i} = V_i \sin\left(\int \omega_i \, dt\right) \tag{3}$$

The inner control is usually composed of a voltage controller and a current controller, in which the reference is the output of the droop controller, denoted as $V_{ref,i} = V_{d,i}$. The control block diagram of the inner loop controller can be equivalent to (4).

$$V_C = V_{ref} \cdot G_V(s) - Z_o(s) \cdot i_o \tag{4}$$

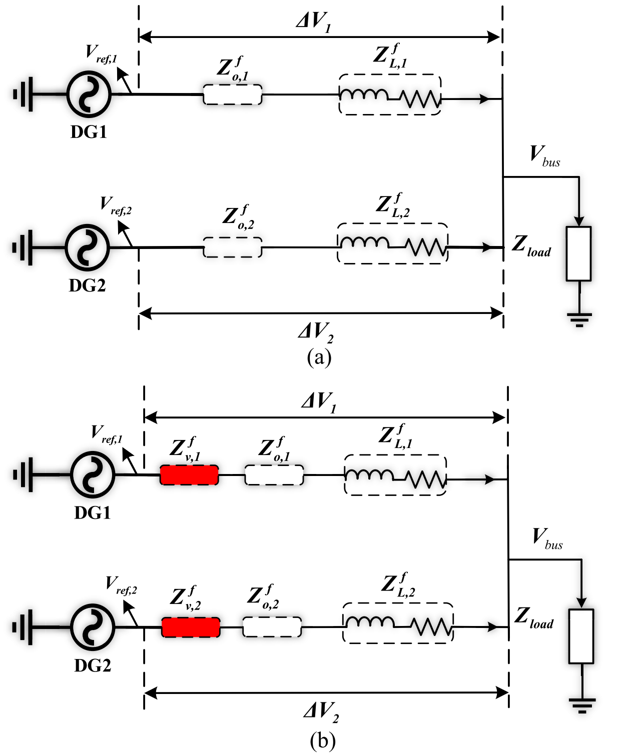

Fig. 3. (a) The effect of feeder mismatch on active power sharing. (b) Virtual impedance on active power control.

where $G_V(s)$ denotes the voltage gain of the inner controller, which should be 1 for a well-designed converter, and $Z_o(s)$ indicates the equivalent impedance of the inverter is determined jointly by the controller's parameters [27] and the droop coefficient.

B. Active Power Analysis

This section investigates how the mismatch impedances of individual *DGs* could contribute to improper active power sharing, as shown in Fig. 3. The voltage drop across the feeder in [17] can be roughly calculated as follows using (5):

$$\Delta V_i \approx \frac{X_i Q_i + R_i P_i}{V_C} \tag{5}$$

where X_i and R_i represent the inductive and resistive components of the feeder and inverter output impedance, ΔV_i denotes the voltage drop.

In Fig. 3, $Z^f_{o,1}$ and $Z^f_{o,2}$ indicate the output impedance. $Z^f_{L,1}$ and $Z^f_{L,2}$ denote the line impedance of feeder 1 and feeder 2, respectively, in Fig. 1. $Z^f_{v,1}$ and $Z^f_{v,2}$ suggest the virtual impedance for active power sharing.

In a resistive feeder systems, $R_i \gg X_i$ [28]. As a result, the power flow through the line resistance leads to the voltage drop, which is expressed as

$$\Delta V_i \approx \frac{R_i P_i}{V_C} \tag{6}$$

Therefore, the voltage drop between the participating units is regulated, and the proportionate sharing of active power is reached by properly modulating individual virtual impedance to be proportional.

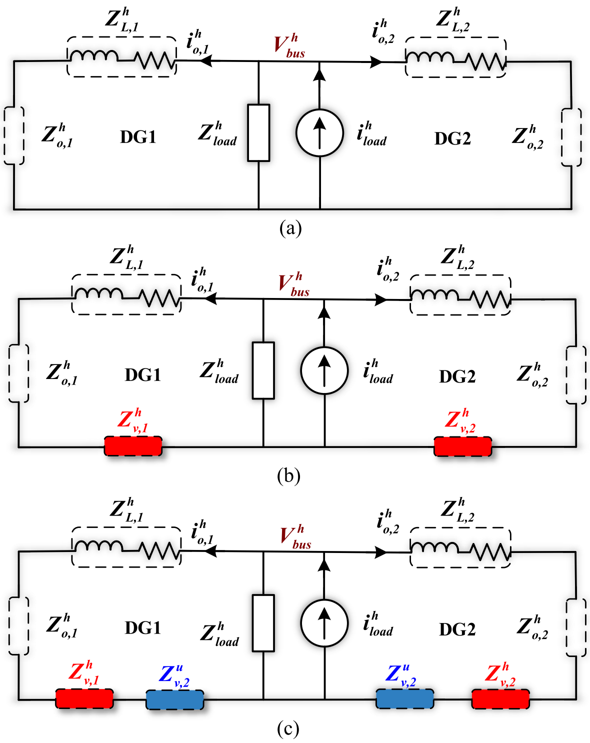

Fig. 4. (a) The effect of feeder mismatch on harmonic current sharing. (b) Virtual impedance on harmonic current control. (c) Virtual impedance on harmonic voltage control.

C. Harmonic Analysis

The following prerequisites must be satisfied for the proportional sharing of harmonic power with its maximum output harmonic power rate.

$$b_1H_1 = b_2H_2 = \cdots = b_iH_i \tag{7}$$

where b_i is the inverse of the maximum output harmonic power. H_i denotes the *h-th* harmonic power. Fig. 4(a) indicates the equivalent circuit of the inverter system at *hth*-order harmonic frequency with a nonlinear load. Note that the nonlinear load can be regarded as a current source i^h_{load} [12]. Where $Z^h_{o,1}$ and $Z^h_{o,2}$ indicate the harmonic output impedance in (4). $Z^h_{L,1}$ and $Z^h_{L,2}$ denote the harmonic line impedance of feeder 1 and feeder 2, respectively, in Fig. 4.

The mismatch of harmonic impedance between $DG1$ and $DG2$ leads to incorrect harmonic power sharing, as illustrated in Fig. 4(a) and Fig. 4(b) as the *hth*-order load harmonic impedance Z^h_{load} is significantly bigger than the equivalent impedance Z^h_{eq} of *DGs*. Nonetheless, by constructing the appropriate virtual harmonic impedance $Z^h_{v,1}$ and $Z^h_{v,2}$, as illustrated in (8), harmonic power sharing could be achieved for selected frequencies.

$$i^h_{o,1}\left(Z^h_{o,1} + Z^h_{v,1} + Z^h_{L,1}\right) = i^h_{o,2}\left(Z^h_{o,2} + Z^h_{v,2} + Z^h_{L,2}\right) \tag{8}$$

D. Bus Voltage Compensation Analysis

The bus voltage is determined by a combination of the harmonic currents produced by the nonlinear load and the equivalent impedance of each inverter. The *h-th* bus harmonic voltage is expressed as (9).

$$V^h_{PCC} = i^h_{o,1}Z^h_{eq,1} = i^h_{o,2}Z^h_{eq,2} \tag{9}$$

where $Z^h_{eq,1}$ and $Z^h_{eq,2}$ represent the equivalent impedance of $DG1$ and $DG2$, including output impedance, line impedance and virtual impedance under *h-th* harmonic current, denoted as $Z^h_{eq,i} = Z^h_{o,i} + Z^h_{v,i} + Z^h_{L,i}$. Eq. (9) demonstrates that it is possible to attenuate the bus voltage harmonic V^h_{PCC} by adjusting the *DGs* virtual impedance for harmonic voltage compensation $Z^u_{v,i}$ as shown in Fig. 4(c).

III. Proposed Impedance Modulation Method

In order to improve bus voltage quality while guaranteeing proportional harmonic power and active power sharing, an adaptive virtual impedance is presented in this paper. Fig. 6 depicts the overall control block diagram, which primarily consists of the communication layer and the virtual impedance of the harmonic power sharing, active power sharing and harmonic voltage compensation loops. By separately adaptively modulating the virtual impedance, the suggested solution reduces the requirement to identify the line impedance. It assumes that each unit needs to share information with the inverters closest to it.

A. Sparse Communication Network

An undirected cyber graph of the communication network is considered to show how the involved converters share data with their neighbours. For every local *ith* converter of the microgrid, the communication graph with all its neighbours-*jth* can be written as a digraph via edges and links via communication adjacency matrix $A = (a_{ij})_{N\times N}$. The communication weight, denoted as a_{ij}, has a value of 1 when there is regular communication between the *i*th unit and the *j*th unit. Conversely, when there is no communication or a communication failure between unit i and unit j, the communication weight is set to 0. The degree of vertex ζ_i is given as $d_i = \sum_{j=1}^{N} a_{ij}.D = diag(d_1, \cdots, d_N)$ is the corresponding degree matrix. Further, the Laplacian matrix L of the communication network L is defined as $L = D - A$. With the sparse communication network outlined above, distributed generation units can communicate with each other to propagate reference information.

B. Harmonic Extract and Power Calculation

In this paper, we use the multi-second-order generalized integrator (SOGI) in [29] to extract fundamental current $i^f_o(t)$, harmonic current $i^h_o(t)$ and harmonic voltage $V^h_{bus}(t)$ as shown in Fig. 5.

The *hth* harmonic power of the *ith* inverter is calculated based on the root mean square (RMS) value $V^f_{i,rms}$ of the fundamental voltage, the RMS value of harmonic current $i^h_{o,irms}$ and its conjugated signal $i^h_{o,d}$ as [30] which can be denoted as (10).

$$H_i = V^f_{i,rms}i^h_{o,irms} = \frac{1}{2}V^f_i\sqrt{i^h_{o,i} + i^h_{o,id}} \tag{10}$$

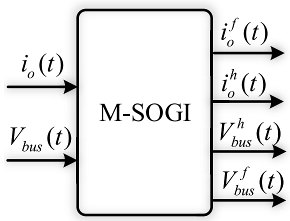

Fig. 5. Comparison of this paper with other studies.

where $V_{i,rms}=V_i/\sqrt{2}$.

C. Consensus-Based Control Method

In Fig. 6, the participating inverters use the communication network to transmit information about active power ($m_{p1}P_1, \cdots, m_{pN}P_N$), harmonic power ($b_1H_1, \cdots, b_NH_N$) and bus voltage distortion rate ($D_1, \cdots, D_N$). Additionally, as was previously noted, reasonable harmonic power sharing cannot match the properly active power sharing and the desired bus voltage quality. Therefore, it is required to independently design the active power sharing controller, harmonic sharing controller and bus voltage compensation controller. The active power controller is established as (11).

$$Z_{v,i}^f = k_{v,i}^f \int \left[\sum_{j\in Ni} a_{ij}\left(m_{pi}P_i - m_{pj}P_j\right) \right] dt \tag{11}$$

The virtual impedance introduced in (12) can be used to share the harmonic power properly.

$$Z_{v,i}^h = k_{v,i}^h \int \left[\sum_{j\in Ni} a_{ij}\left(b_iH_i - b_jH_j\right) \right] dt \tag{12}$$

Unlikely in [22], decreasing the overall impedance for PCC voltage quality improvement, which potentially causes instability, we have implemented a voltage compensation loop. The bus harmonic voltage compensation controller is written as (13).

$$Z_{v,i}^u = k_{v,i}^u \int \left[\sum_{j\in Ni} a_{ij}\left(D_j - D_i\right) + g_i(D_0 - D_i) \right] dt \tag{13}$$

where the integral controllers are employed to eliminate active and harmonic power-sharing errors. The loop gain g_i=1 is a pinning gain for the harmonic voltage compensation controller. $k_{v,i}^f$, $k_{v,i}^h$ and $k_{v,i}^u$ are the impedance reshaping factors for active power sharing, harmonic power sharing and harmonic voltage compensation, respectively. The details of parameter selection are given in Section IV-C. The D_0 is the maximum allowable harmonic voltage distortion rate. D_i denotes the *hth* order harmonic distortion of *ith* unit as (14).

$$D_i = \frac{V_i^h}{V_i^f} \tag{14}$$

In Fig. 5, V_i^f and V_i^h represent the fundamental voltage and *h-th* harmonic voltage, respectively. It is worth noting that the capacitor voltage is used in place of the PCC voltage due to the small line impedance in low-voltage grids. If the harmonic voltage exceeds the permissible distortion limits or the active and harmonic power may not be shared correctly, the virtual impedance is automatically adjusted to be the desired value in such a scenario.

With the virtual impedance reshaping loops, the voltage reference of the double-loop voltage controller is obtained as (15):

$$V_{ref} = V_d - Z_v^f i_o^f - Z_v^h i_o^h - Z_v^u i_o^h \tag{15}$$

It should be noted that excessively low virtual impedance can lead to unstable operation due to the potential occurrence of circulating current among the inverters involved. Meanwhile, an excessively high virtual impedance can result in poor PCC voltage quality. This study's overall impedance encompasses the line impedance, output impedance (modelled by the inner controller), and virtual impedance. The initial impedance (line impedance and output impedance) is predetermined once the system is established, and they typically exhibit relatively large initial values. Consequently, the virtual impedance is adjusted to compensate for the initial impedance. It is worth noting that even if the virtual impedance (resistance) has a negative value, the overall impedance (resistance) will still be positive and sufficiently large to ensure the system's stability. Furthermore, the feeder investigated in this paper is primarily resistive, employing a resistive virtual impedance. Unlike inductive scenarios, this characteristic contributes to the system's enhanced stability as it avoids differential terms. Furthermore, when the sum of the output impedance and line impedance becomes negligibly small, it becomes necessary to introduce an additional fixed virtual impedance to maintain a sufficiently substantial initial impedance, thus preserving system stability [31].

IV. Cyber Attack and Stability Analysis

Communication-based methods help guarantee that the fundamental and harmonic impedances are set appropriately but are susceptible to cyber-attacks. This section initially describes and models the false data injection attack (FDIA). Next, we develop a strategy for the FDIA to challenge convergence performance. On top of that, the auxiliary controllers, designed to enhance resilience, can resist cyber-attacks carried through the communication network, and it is immunized to communication failure and delay. Furthermore, remain aware that only at the first stage of system construction does the controller exchange data with its neighbours. After which, the introduced auxiliary controller sends the communication network disabled signal to participated units, while the microgrid can maintain the desired power-sharing performance and PCC harmonic voltage quality without further communication. As a result, the communication burden is significantly reduced.

A. Cyber Attack Problem Statement

The attack that draws the greatest attention is FDIA. It can be thought of as fake data modelled as in (16) and then injected into the actual data.

$$x_{a,j} = x_j + \eta_j \varepsilon(t) \tag{16}$$

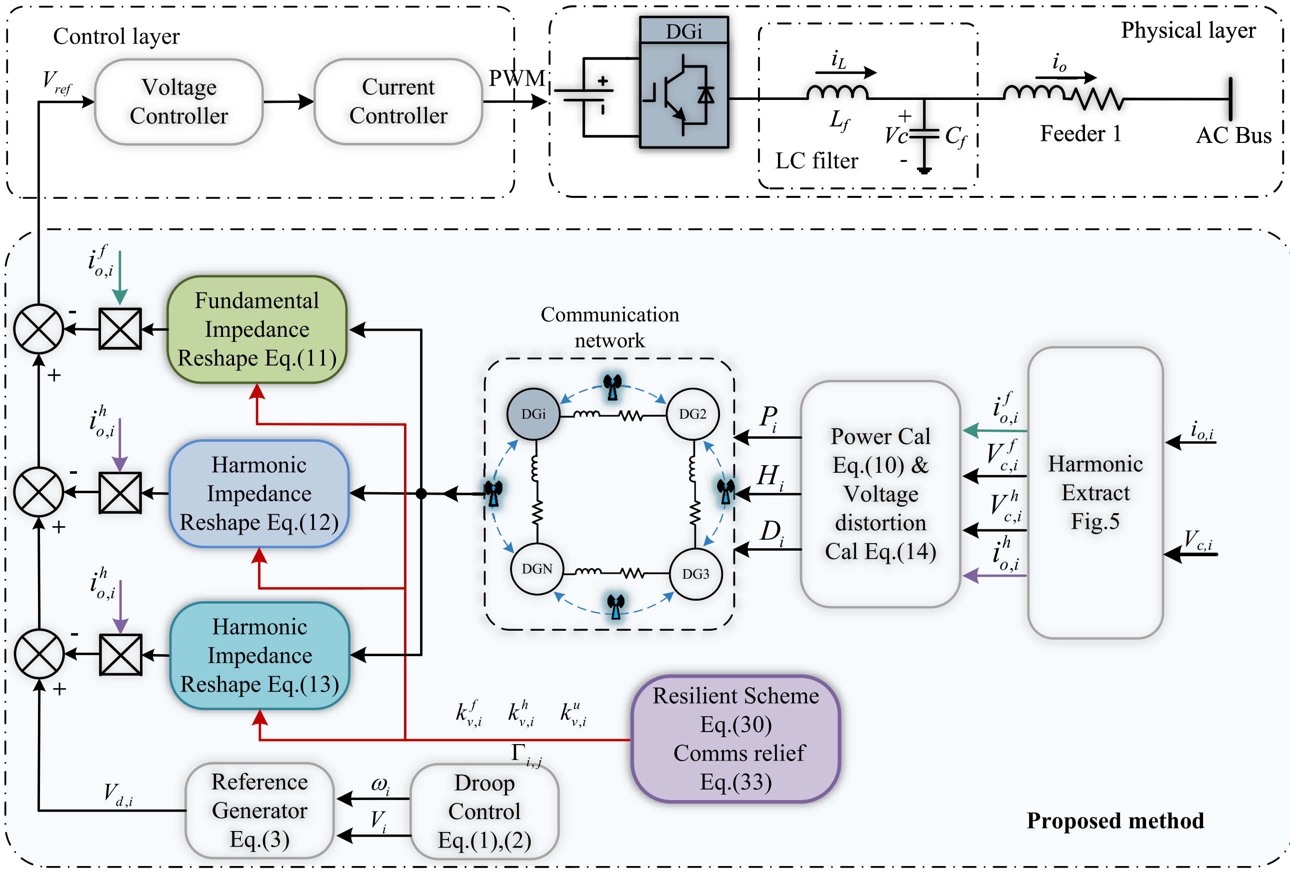

Fig. 6. The proposed virtual impedance framework.

where $x_{a,j}$ denotes the information from the attacked neighbouring unit, and x_j gives the actual information. The binary variable termed η_j indicates the presence of FDIA with the malicious element $\varepsilon(t)$ when $\eta_j = 1$ stands for the presence of an attack and $\eta_j = 0$ indicates the absence of FDIA.

For active power sharing controller: We can intuitively develop the expression $P_i = H_L^f/(Z_{v,i}^f + Z_{o,i}^f + Z_{L,i}^f)$, as shown in Fig. 3, where H_L^f a represents the positive term between impedance and active power derived from (8). Considering the presence of FDIA on the communication network, the proposed method in (11) can be expressed as in (17).

$$\frac{H_L^f}{P_i} = k_{v,i}^f \sum_{j\in Ni} a_{ij}\big(n_{pi}P_i - n_{pj}P_{a,j}\big)dt + Z_{o,i}^f + Z_{L,i}^f \quad (17)$$

The state error e_i^f, which is expected to be 0, is defined as the differences between the *ith* inverter's active power and its optimal value, denoted as $e_i^f = n_{pi}P_i - P_0$. Where P_0 represents the optimal output active power of *ith* inverter. In the steady state, $n_{p1}P_1 = \cdots = n_{pi}P_i = P_0$. The dynamics of state errors with attacks on communication links are stated as follows:

$$e_i^f(t) = \frac{H_L^f}{\int\Big[-k_{v,i}^f Le_i^f + B\varepsilon(t)\Big]dt + Z_{o,i}^f + Z_{L,i}^f} - P_0 \quad (18)$$

where L is the Laplacian matrix of the communication network. B is the incidence matrix of cyber attack and output. The derivative of the state errors can be written as (19):

$$\dot{e}_i^f(t) = \frac{-H_L^f k_{v,i}^f Le_i^f + B\varepsilon(t)}{\{\int\Big[-k_{v,i}^f Le_i^f + B\varepsilon(t)\Big]dt + Z_{o,i}^f + Z_{L,i}^f\}^2} \quad (19)$$

For the harmonic power sharing controller: As shown in Fig. 4, we can develop the expression $H_i = H_L^h/(Z_{v,i}^h + Z_{o,i}^h + Z_{L,i}^h)$, where H_L^h is a positive term, denotes the inverse of impedance and harmonic power. Considering the presence of FDIA on the communication network and corresponding to (20), we can obtain the following:

$$\frac{H_L^h}{H_i} = \int k_{v,i}^h [\sum_{j\in Ni} a_{ij}(b_i H_i - b_j H_{a,j}]dt + Z_{o,i}^h + Z_{L,i}^h \quad (20)$$

The state error for harmonic power sharing is $e_i^h = b_i H_i - H_0$, where H_0 represents the optimal harmonic power of *ith* inverter. In the steady state, $b_1 H_1 = \cdots = b_i H_i = H_0$. The dynamics of state errors with attacks on communication links are stated as follows:

$$e_i^h(t) = \frac{H_L^h}{\int\big[-k_{v,i}^h Le_i^h + B\varepsilon(t)\big]dt + Z_{o,i}^h + Z_{L,i}^h} - H_0 \quad (21)$$

The derivative of the state errors can be written as (22):

$$\dot{e}_i^h(t) = \frac{-H_L^h k_{v,i}^h Le_i^h + B\varepsilon(t)}{\{\int\big[-k_{v,i}^h Le_i^h + B\varepsilon(t)\big]dt + Z_{o,i}^h + Z_{L,i}^h\}^2} \quad (22)$$

For the voltage compensation controller: As shown in Fig. 4, we can intuitively develop the expression $D_i = H_L^u(Z_{o,i}^h + Z_{L,i}^h + Z_{vH,i}^h + Z_{vV,i}^h)$ where $H_L^u = i_{o,i}^h / V_{bus}^f$. Considering the presence of FDIA on the communication network and corresponding to (13), we can obtain the following:

$$\frac{D_i}{H_L^u} = k_{v,i}^u \int \left[\sum_{j \in Ni} a_{ij}(D_{a,j} - D_i) + g_i(D_0 - D_i) \right] dt + Z_{eq,i}^h \tag{23}$$

As the state error is defined as $e_i^v(t) = D_i - D_0^h$. It can be represented as follows:

$$e_i^u(t) = \int \left[-H_L^u k_{v,i}^u (L+G) e_i^u + B\varepsilon(t) \right] dt + Z_{eq,i}^h \tag{24}$$

where $G = diag(g_1, \ldots, g_N)$. The derivative of the state error can be written as (25)

$$\dot{e}_i^u(t) = -H_L^u k_{v,i}^u (L+G) e_i^u + B\varepsilon(t) \tag{25}$$

B. Stability Analysis

To analyse the stability, the Lyapunov function is defined as:

$$\nu(e) = \frac{1}{2} e^T e \tag{26}$$

where e represents the state error e_i^f, e_i^h and e_i^u of the proposed controllers. The time derivative of $\nu(e)$ along the trajectories (26) of different controller is calculated as follows:

$$\begin{aligned} \dot{\nu}(e) &= e^T \dot{e} \\ &= \begin{cases} (e_i^f)^T \dfrac{-H_L^f k_{v,i}^f L e_i^f + B\varepsilon(t)}{\{\int \left[-k_{v,i}^f L e_i^f + B\varepsilon(t) \right] dt + Z_{o,i}^f + Z_{L,i}^f\}^2} \\ (e_i^h)^T \dfrac{-H_L^h k_{v,i}^h L e_i^h + B\varepsilon(t)}{\{\int \left[-k_{v,i}^h L e_i^h + B\varepsilon(t) \right] dt + Z_{o,i}^h + Z_{L,i}^h\}^2} \\ (e_i^u)^T \left[-H_L^u k_{v,i}^u (L+G) e_i^u + B\varepsilon(t) \right] \end{cases} \end{aligned} \tag{27}$$

In Eq. (27), in the absence of cyber attacks, which means $B\varepsilon(t) = 0$ and $\dot{\nu}(e) < 0$ for all $e \neq 0$ in the steady state. As a result, eq. (11), (12), and (13) are globally asymptotically stable. Consequently, $\nu(e)$ will eventually converge to zero, leading to the convergence of state error to zero and ensuring that the active and harmonic power can be proportionally shared. Additionally, the harmonic voltage will be reduced to the desired value.

When the system is attacked by FDIA with malicious signal $\varepsilon(t)$, we develop a new state variable y_i, where $y = e - \varepsilon(t)$. With the same Lyapunov function with (26), The derivative of $\nu(y)$ can be written as (28).

$$\begin{aligned} \dot{\nu}(y) &= y^T \dot{y} \\ &= \begin{cases} (y_i^f)^T \dfrac{-H_L^f k_{v,i}^f L y_i^f}{\{\int \left[-k_{v,i}^f L y_i^f \right] dt + Z_{o,i}^f + Z_{L,i}^f\}^2} \\ (y_i^h)^T \dfrac{-H_L^h k_{v,i}^h L y_i^h}{\{\int \left[-k_{v,i}^h L y_i^h \right] dt + Z_{o,i}^h + Z_{L,i}^h\}^2} \\ (y_i^u)^T \left[-H_L^u k_{v,i}^u (L+G) y_i^u \right] \end{cases} \end{aligned} \tag{28}$$

In (28), it can be observed that $\dot{\nu}(y) < 0$ for all $y \neq 0$ in the steady state. Consequently, $\nu(y)$ will eventually converge to zero, leading to the convergence of state error to zero. This implies that $y = 0$ and $e = \varepsilon(t)$ impede power-sharing and harmonic voltage compensation.

C. Resilient Framework and Communication Relief Controller

In this paper, we propose a resilient enhanced auxiliary controller to suppress cyber-attacks.

The proposed resilience scheme for mitigating cyber attacks that impede virtual impedance convergence can be rewritten as (29).

$$Z_{v,i} = \pm k_{v,i} \int \left[\sum_{j \in Ni} a_{ij}(x_i - x_j) + g_i(x_i - x_0) \right] dt \tag{29}$$

where $Z_{v,i}$, $k_{v,i}$ and x_i represent the virtual impedance, reshape factor and state variable in (11), (12) and (13). "$\pm$" denotes the different Laplacian matrix of the communication network.

If we take $\Delta\delta_{i,j} = x_j - x_i$. $\Delta\delta'_{i,j}$ can be taken as follows to replace the original data:

$$\Delta\delta'_{i,j} = (1 - \Gamma_{i,j})\Delta\delta_{i,j} \tag{30}$$

where $\Gamma_{i,j}$ is a binary variable, representing the existence of a cyber attack or not.

$$\Gamma_{i,j} = \begin{cases} 1, & if\ |\Psi_{i,j}| \geq \Upsilon_i \\ 0, & else \end{cases} \tag{31}$$

We adopt $\Psi_{i,j}$ to identify the cyber attack, which can be written as (32). Υ_i denotes the cyber attack measure threshold. It is defined as $\Upsilon_i = 0.01x_i$ in this paper. If $|\Psi_{i,j}| \geq \Upsilon_i$, $\Gamma_{i,j} = 1$, it is suggested there is a cyber attack or else indicating no cyber attack in the system.

$$\Psi_{i,j} = a_{ij}(x_i - x_j) \tag{32}$$

If a cyber attack occurs between the *jth* DG unit and *ith* DG unit, the binary signal $\Gamma_{i,j}$ is sent to isolate the corrupted data; thus, the infected data is disregarded. Consequently, the proposed communication-based strategy is immune to cyber-attacks with the procedure in the resilient framework.

The auxiliary controller used for disabling the proposed method to decrease the communication burden that can be expressed as follows:

$$k_{v,i} = \begin{cases} k_{v,i}, & if \quad \Gamma_{i,1} \cup \Gamma_{i,2} \cdots \cup \Gamma_{i,N} = 0 \\ 0, & else \end{cases} \tag{33}$$

The reshape factors $k_{v,i}$ determine the convergence speed of the outer loop. Increasing the value of these factors enhances communication efficiency among the inverters involved. However, in the case of the virtual impedance loop, the reshape factors should be set at a slower rate than the inner loop. Additionally, since the virtual impedance is calculated based on power, it should have an even slower convergence rate than the power loop. To ensure this, as the cutoff angular frequency of the power loop's filter is set at 100 rad/s, the reshape factors are selected as 0.02.

When the inverter system has been built with the proposed method, it is assumed the harmonic and active power can be proportionally shared alone with harmonic voltage within

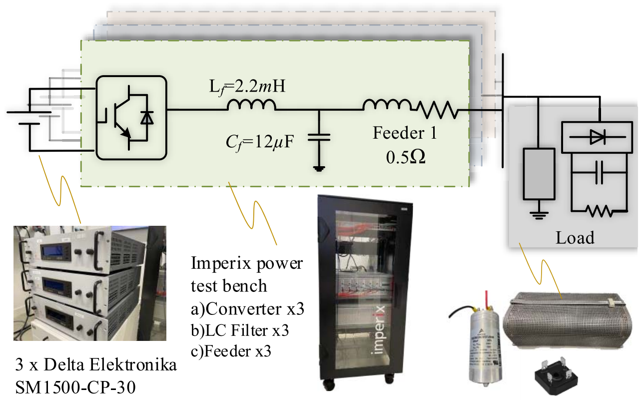

Fig. 7. Experiment setup.

TABLE I
PARAMETERS OF THE MICROGRID IN EXPERIMENT

Symbol	Interpretation	Value
U_{dc}	DC-link voltage	150V
Z_L	Line impedance	0.5Ω
L_f	Inductor of LC filter	2.2mH
C_f	Capacitor of LC filter	12μF
f_s	Switch frequency	20kHz
m_{P1}, n_{Q1}	Droop coefficient of $DG1$	1/1000
m_{P2}, n_{Q2}	Droop coefficient of $DG2$	1/2000
m_{P3}, n_{Q3}	Droop coefficient of $DG3$	1/3000
k_{ph}	Proportional coefficient	0.001
k_{rh}	resonant coefficient	50
$k_{v,i}$	reshape factor	0.02
ω^*	Nominal angular frequency	314rad/s
V^*	Nominal voltage amplitude	110V

the acceptable range. In this case, the auxiliary controller triggered, resulting in the impedance reshaping factor $k_{v,i}$=0, rendering the microgrid independent of communication.

V. EXPERIMENT RESULTS

The proposed adaptive control strategy has been tested in experiments of a distributed AC micro-grid with three inverters connected in parallel to validate its effectiveness, as shown in Fig. 7. In this microgrid system, the output side of the inverters is connected to the AC bus through an LC filter and line impedance.

Following the structure in Fig. 7, several cases are carried out in this paper to verify the effectiveness of the proposed adaptive control scheme with different operations. The plant and control parameters of the microgrid are provided in Table I. In this paper, the 3^{rd} harmonic is selected as an example for verifying. the inverters' output harmonic and active power rate follows the maximum capacity proportion set as 1:2:3. The PCC harmonic voltage disordered rate should be below 5%, which complies with the IEEE 519-1992 standard harmonic distortion rate restriction [32].

A. Active and Harmonic Power Sharing

Fig. 8 illustrates the performance of the proposed method. Initially, as shown in Fig. 8 (a) and (b), conventional droop control is used to regulate the microgrids after the system

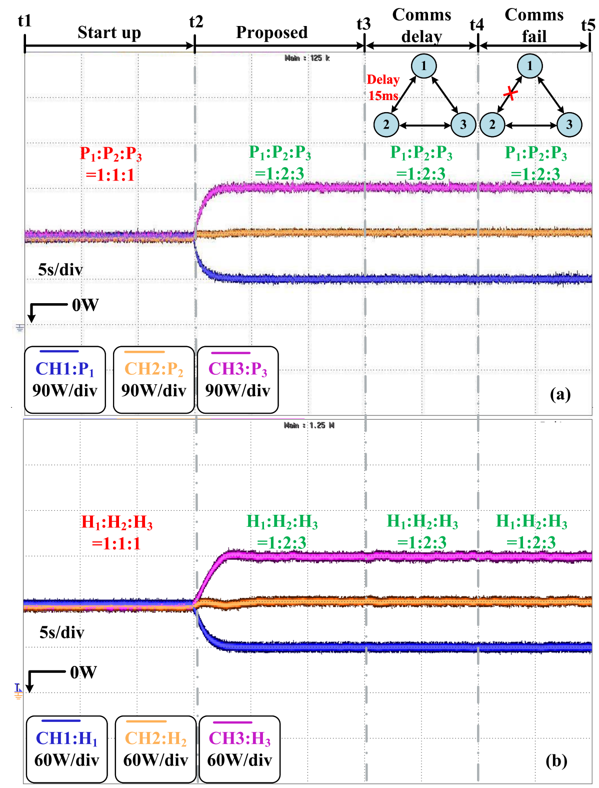

Fig. 8. Power sharing performance of the proposed controller: (a) active power. (b) 3^{rd} harmonic power.

starts at t1, resulting in an improper power-sharing ratio of 1:1:1. At t2, the proposed adaptive virtual impedance is activated, contribute to a proportional sharing of active power and 3^{rd} harmonic power with the desired ratio of 1:2:3. The effectiveness of the proposed communication-based virtual impedance is further demonstrated by intentionally imposing communication delays (15ms) and interruptions in the communication link from $DG2$ to $DG1$ at t3 and t4, respectively. Despite these disruptions, the system response exhibits no significant changes during these periods, confirming the proposed method's immunity to communication delays and interruptions. The determination of an upper bound on communication delay can be achieved through the utilization of Riccati equation-based analysis, as detail demonstrated in [33]. Consequently, the time delay specified in this study amounts to 15ms for the network. However, since the delay analysis is not the main contribution of this paper and in the interest of brevity, this analysis has been omitted from the current paper.

B. Cyber Attack and Resilience Enhancement

Fig. 9 (a) and (b) demonstrate the impact of cyber attacks on microgrids and the effectiveness of the proposed method in mitigating such attacks. In the t2-t6 stage, the adaptive virtual impedance is adopted. Therefore, the active and harmonic power can be proportional sharing, and there is no cyber attack in the communication network. Subsequently, the communication line from $DG2$ to $DG1$ is subject to a

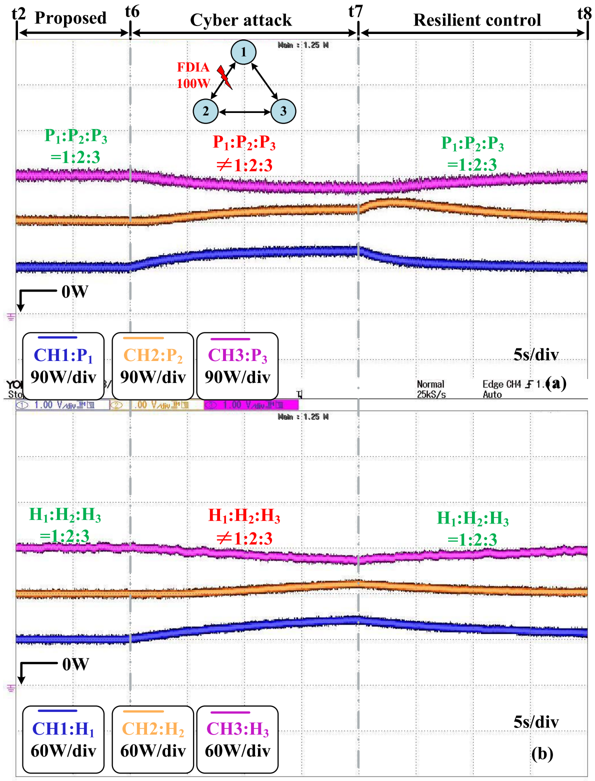

Fig. 9. Effect of cyber attack and performance of the resilient controller: (a) active power. (b) 3^{rd} harmonic power.

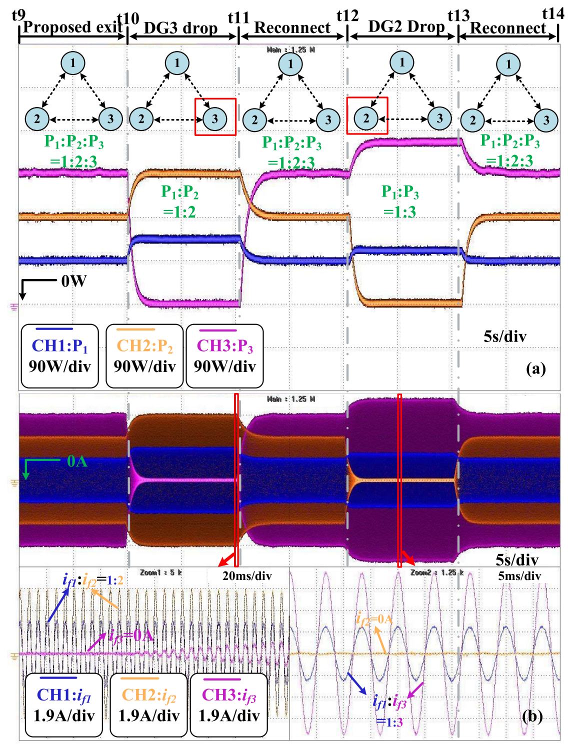

Fig. 10. The plug-and-play operation for the active power controller after communication is disabled: (a) active power. (b) fundamental current.

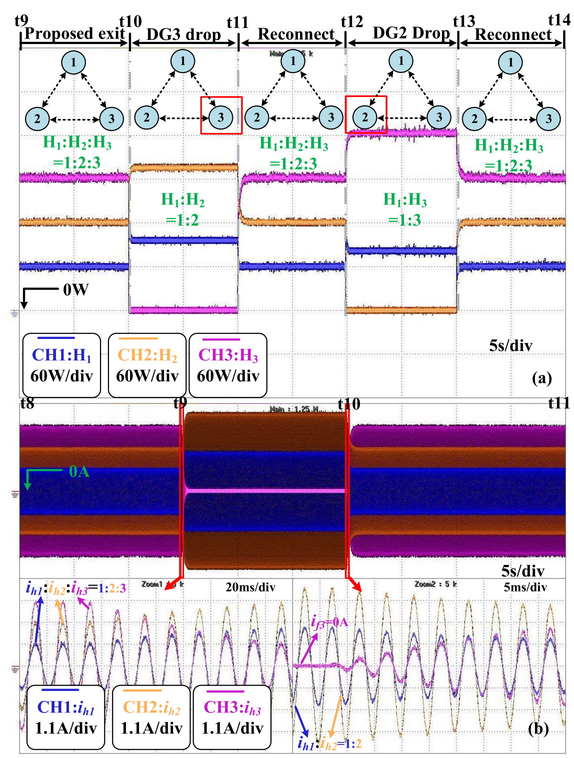

Fig. 11. The plug-and-play operation for the harmonic power controller after communication is disabled: (a) 3^{rd} harmonic power. (b) 3^{rd} harmonic current.

false data injection attack with $\varepsilon(t) = 100$ W for both active power and harmonic power controllers at t6. As a result, the power-sharing ratio deviates from the optimal point. At t7, the proposed resilient framework is activated, eliminating the corrupted data and recovering the power-sharing ratio to 1:2:3. The results demonstrate the resilience of the proposed method against cyber-attacks, highlighting its potential for enhancing the security and stability of microgrids.

C. Communication Relief Strategy

The limited communication resource constraints the wide use of distributed control. This paper proposes a communication relief control to alleviate the communication burden by disabling the communication-based virtual impedance after the system is built up. Moreover, it is necessary to keep sharing accuracy among the operational units when one DG unit drops. This paper tests the active and harmonic power in the plug-and-play operation after the communication-based method exit. Fig. 10(a),(b) show the performance of active power and fundamental current, while where Fig. 11(a),(b) show the performance of harmonic power and 3^{rd} harmonic current, respectively.

As shown in Fig. 10(a) and Fig. 11(a), the communication-based control strategy terminates at t9, allowing the active and harmonic power to continue to be shared proportionally without communication support. While before t9, the inverter is regulated by the proposed communication-based virtual impedance. At t10, $DG3$ disconnects, while the operational $DG1$ and $DG2$ maintain a power-sharing ratio of 1:2. at t12, $DG2$ drops out, and the operational $DG1$ and $DG3$maintain a power-sharing ratio of 1:3. In both cases,

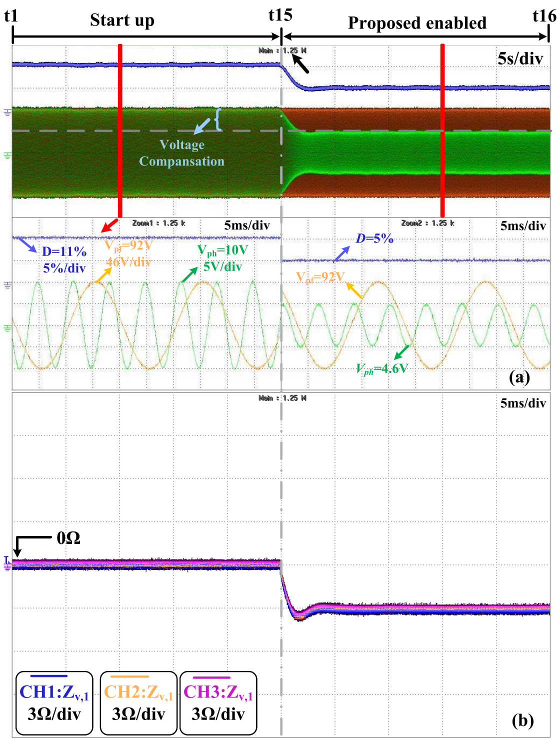

Fig. 12. The validity of PCC harmonic voltage compensation: (a) PCC voltage. (b) virtual impedance waveform.

the system operates reliably and accurately without the need for communication-based control. During periods t11-t12 and t13-t14, the disconnected unit is reconnected, and the system returns to its original configuration with proportional power-sharing.

The fundamental waveform in Fig. 10(b) demonstrates consistent and accurate fundamental current sharing throughout the operation. Fig. 11(b) presents the 3^{rd} harmonic current of two dynamic processes. 1) when $DG3$ drop out at t9, the harmonic current sharing ratio is changed from 1:2:3 to 1:2:0 among $DG1$: $DG2$:$DG3$. 2) when $DG3$ is reconnected to the microgrid at t10. the harmonic output current of $DG3$ is increased and, eventually, keeps proportional sharing among the involved inverter.

Following the information exchange during the build-up stage via the communication network, the virtual impedance is modulated to the desired value and remains constant during the whole process due to the integrator effect of the proposed method. As a result, even when the communication network is disabled, the active and harmonic power can still be proportionally shared, and importantly, the microgrid remains the plug-and-play operation at this stage.

D. Harmonic Voltage Compensation

To evaluate the effectiveness of the proposed control for compensating harmonic voltage distort rate and the sensitivity of PCC harmonic voltage with respect to virtual impedance, a comparison is developed between the waveforms obtained before and after the implementation of the proposed method, as illustrated in Fig. 12. In the t1-t15 stage, the harmonic distortion rate, represented by D, is 10%, with the fundamental voltage measured at 98V and the 3^{rd} harmonic voltage at 10V. Subsequently, at t15, the proposed method is employed, attenuating the 3^{rd} harmonic impedance. Consequently, the harmonic distortion rate D decreases to 5%, the 3^{rd}harmonic voltage shifts to 5V, while the fundamental voltage remains unchanged, which validates the effectiveness of the proposed method for harmonic voltage mitigation.

As elaborated in Section II, PCC harmonic voltage exhibits a positive relationship with virtual impedance, as shown in Fig. 12(b). Therefore, the reduction in harmonic impedance of the involved inverters leads to a decrease in the distorted rate of harmonic voltage as the drop in harmonic voltage diminishes.

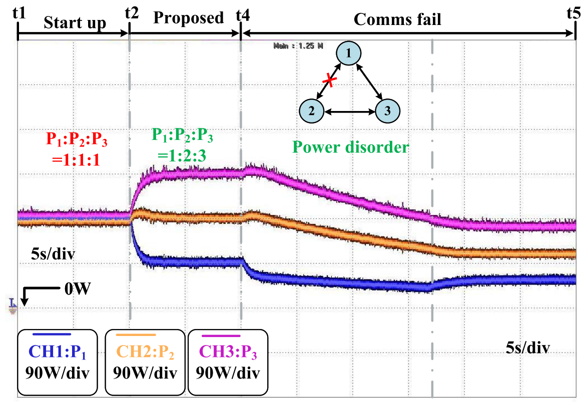

Fig. 13. Active power sharing performance with the method in [12], [17].

E. Comparative Study

To illustrate the advantages of the proposed method in this paper, a comparative analysis was conducted, as depicted in Fig. 13 and Fig. 14, showcasing the active power performance.

Fig. 13 illustrates the active power performance when the communication link fails using the secondary method introduced in [12], [17]. After activating the secondary control mechanism at time t2, the power-sharing ratio transitioned from 1:1:1 to 1:2:3. At t4, a communication failure occurs within the 2-1 link, inducing a disordered power reference signal and system power output. It should be noted that the persistent steady-state condition observed during the communication failure is attributable to constraints imposed on the system output to protect the experimental setup. Although the power-sharing ratio remains 1:2:3 during this period, the output power is reduced. As indicated in Fig. 8 and Fig. 13, it becomes evident that utilising the secondary control approach proposed in [12], [17] potentially gives rise to power distortions under communication failure scenarios. This distortion, however, can be eliminated by applying the proposed virtual impedance method introduced in this paper.

Fig. 14 indicates the active power performance with the secondary control introduced in [11], [18], under the communication link disabled. It is worth noting that during the period from t10 to t11, DG3 drops out, resulting in an active power allocation ratio between DG1 and DG2 inconsistent with the expected 1:2 ratio. In addition, in another period, t12-t13, DG2 drops out, and the active power-sharing correlation between

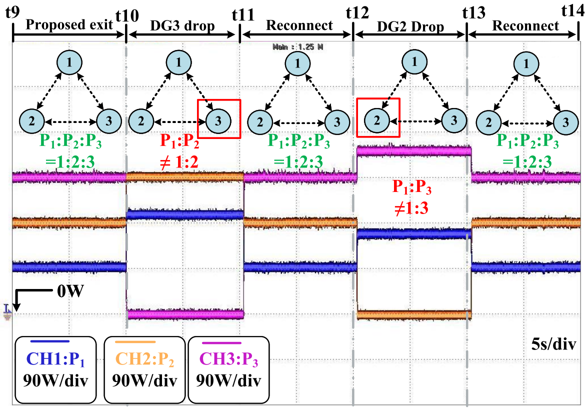

Fig. 14. Active power sharing performance with the method in [11], [18] after communication is disabled.

DG1 and DG3 deviates from the expected 1:3 ratio. This illustrates the necessary role of communication in the secondary control described in [11], [18], which imposes a heavy communication burden on the microgrid system. In contrast, the proposed novel approach in this manuscript alleviates the communication burden since the microgrid keeps plug-and-play operation even without communication, as evidenced by the study results in Fig. 10 and Fig. 11.

VI. Conclusion

This paper proposes an adaptively adjusted virtual impedance method contributing to accurate active and harmonic power sharing. Moreover, it interacts only with neighbouring units during the system construction phase, significantly reducing communication time with ensuring plug-and-play operation. An auxiliary controller is also employed to isolate corrupted data, thereby enhancing system resilience against cyber-attacks and communication disruptions. Furthermore, the harmonic voltage compensation controller ensures that PCC voltage harmonic distortion remains within 5%. The experimental results verify the performance of the proposed control scheme.

References

[1] A. R. Jordehi, "Allocation of distributed generation units in electric power systems: A review," *Renew. Sustain. Energy Rev.*, vol. 56, pp. 893–905, Apr. 2016.

[2] Y. Han, H. Li, P. Shen, E. A. A. Coelho, and J. M. Guerrero, "Review of active and reactive power sharing strategies in hierarchical controlled microgrids," *IEEE Trans. Power Electron.*, vol. 32, no. 3, pp. 2427–2451, Mar. 2017.

[3] J. M. Guerrero, L. G. De Vicuna, J. Matas, M. Castilla, and J. Miret, "Output impedance design of parallel-connected UPS inverters with wireless load-sharing control," *IEEE Trans. Ind. Electron.*, vol. 52, no. 4, pp. 1126–1135, Aug. 2005.

[4] J. Xiao, Y. Jia, B. Jia, Z. Li, Y. Pan, and Y. Wang, "An inertial droop control based on comparisons between virtual synchronous generator and droop control in inverter-based distributed generators," *Energy Rep.*, vol. 6, pp. 104–112, Dec. 2020.

[5] Z. Qin, L. Wang, and P. Bauer, "Review on power quality issues in EV charging," in *Proc. IEEE 20th Int. Power Electron. Motion Control Conf. (PEMC)*, 2022, pp. 360–366.

[6] L. Wang, Z. Qin, T. Slangen, P. Bauer, and T. Van Wijk, "Grid impact of electric vehicle fast charging stations: Trends, standards, issues and mitigation measures—An overview," *IEEE Open J. Power Electron.*, vol. 2, pp. 56–74, 2021.

[7] H. Han, X. Hou, J. Yang, J. Wu, M. Su, and J. M. Guerrero, "Review of power sharing control strategies for islanding operation of AC microgrids," *IEEE Trans. Smart Grid*, vol. 7, no. 1, pp. 200–215, Jan. 2016.

[8] J. Chen, L. Wang, L. Diao, H. Du, and Z. Liu, "Distributed auxiliary inverter of urban rail train—Load sharing control strategy under complicated operation condition," *IEEE Trans. Power Electron.*, vol. 31, no. 3, pp. 2518–2529, Mar. 2016.

[9] T. V. Hoang and H.-H. Lee, "Accurate power sharing with harmonic power for islanded multibus microgrids," *IEEE J. Emerg. Sel. Topics Power Electron.*, vol. 7, no. 2, pp. 1286–1299, Jun. 2019.

[10] H. Mahmood, D. Michaelson, and J. Jiang, "Accurate reactive power sharing in an islanded microgrid using adaptive virtual impedances," *IEEE Trans. Power Electron.*, vol. 30, no. 3, pp. 1605–1617, Mar. 2015.

[11] J. W. Simpson-Porco, Q. Shafiee, F. Dörfler, J. C. Vasquez, J. M. Guerrero, and F. Bullo, "Secondary frequency and voltage control of islanded microgrids via distributed averaging," *IEEE Trans. Ind. Electron.*, vol. 62, no. 11, pp. 7025–7038, Nov. 2015.

[12] Z. Wang et al., "Adaptive harmonic impedance reshaping control strategy based on a consensus algorithm for harmonic sharing and power quality improvement in microgrids with complex feeder networks," *IEEE Trans. Smart Grid*, vol. 13, no. 1, pp. 47–57, Jan. 2022.

[13] Y. Fan, G. Hu, and M. Egerstedt, "Distributed reactive power sharing control for microgrids with event-triggered communication," *IEEE Trans. Control Syst. Technol.*, vol. 25, no. 1, pp. 118–128, Jan. 2017.

[14] J. Zhou, S. Kim, H. Zhang, Q. Sun, and R. Han, "Notice of Removal: Consensus-based distributed control for accurate reactive, harmonic, and imbalance power sharing in microgrids," *IEEE Trans. Smart Grid*, vol. 9, no. 4, pp. 2453–2467, Jul. 2018.

[15] L. Meng et al., "Distributed voltage unbalance compensation in islanded microgrids by using a dynamic consensus algorithm," *IEEE Trans. Power Electron.*, vol. 31, no. 1, pp. 827–838, Jan. 2016.

[16] X. Lu, X. Yu, J. Lai, J. M. Guerrero, and H. Zhou, "Distributed secondary voltage and frequency control for islanded microgrids with uncertain communication links," *IEEE Trans. Ind. Informat.*, vol. 13, no. 2, pp. 448–460, Apr. 2017.

[17] J. Lu, M. Savaghebi, B. Zhang, X. Hou, Y. Sun, and J. M. Guerrero, "Distributed dynamic event-triggered control for accurate active and harmonic power sharing in modular on-line UPS systems," *IEEE Trans. Ind. Electron.*, vol. 69, no. 12, pp. 13045–13055, Dec. 2022.

[18] J. Xiao, L. Wang, Z. Qin, and P. Bauer, "A resilience enhanced secondary control for AC micro-grids," *IEEE Trans. Smart Grid*, early access, Apr. 18, 2023, doi: 10.1109/TSG.2023.3268245.

[19] J. M. Guerrero, J. Matas, L. G. de Vicuna, M. Castilla, and J. Miret, "Decentralized control for parallel operation of distributed generation inverters using resistive output impedance," *IEEE Trans. Ind. Electron.*, vol. 54, no. 2, pp. 994–1004, Apr. 2007.

[20] J. Xiao, L. Wang, Z. Qin, and P. Bauer, "Detection of cyber attack in smart grid: A comparative study," in *Proc. IEEE 20th Int. Power Electron. Motion Control Conf. (PEMC)*, 2022, pp. 48–54.

[21] B. Liu, Z. Liu, J. Liu, R. An, H. Zheng, and Y. Shi, "An adaptive virtual impedance control scheme based on small-AC-signal injection for unbalanced and harmonic power sharing in islanded microgrids," *IEEE Trans. Power Electron.*, vol. 34, no. 12, pp. 12333–12355, Dec. 2019.

[22] P. Sreekumar and V. Khadkikar,, "A new virtual harmonic impedance scheme for harmonic power sharing in an islanded microgrid," *IEEE Trans. Power Del.*, vol. 31, no. 3, pp. 936–945, Jun. 2016.

[23] M. S. Sadabadi, S. Sahoo, and F. Blaabjerg, "A fully resilient cyber-secure synchronization strategy for AC microgrids," *IEEE Trans. Power Electron.*, vol. 36, no. 12, pp. 13372–13378, Dec. 2021.

[24] X.-K. Liu, S.-Q. Wang, M. Chi, Z.-W. Liu, and Y.-W. Wang, "Resilient secondary control and stability analysis for DC microgrids under mixed cyber attacks," *IEEE Trans. Ind. Electron.*, vol. 71, no. 2, pp. 1938–1947, Feb. 2024.

[25] J. Xiao, L. Wang, Z. Qin, and P. Bauer, "An adaptive cyber security scheme for AC micro-grids," in *Proc. IEEE Energy Convers. Congr. Expo. (ECCE)*, 2022, pp. 1–6.

[26] C. Zhao, J. He, P. Cheng, and J. Chen, "Consensus-based energy management in smart grid with transmission losses and directed communication," *IEEE Trans. Smart Grid*, vol. 8, no. 5, pp. 2049–2061, Sep. 2017.

[27] L. B. Larumbe, Z. Qin, L. Wang, and P. Bauer, "Impedance modeling for three-phase inverters with double synchronous reference frame current controller in the presence of imbalance," *IEEE Trans. Power Electron.*, vol. 37, no. 2, pp. 1461–1475, Feb. 2022.

[28] J. Xiao, L. Wang, Z. Qin, and P. Bauer, "Virtual impedance control for load sharing and bus voltage quality improvement," in *Proc. 25th Eur. Conf. Power Electron. Appl. (EPE ECCE Europe)*, 2023, pp. 1–8.

[29] P. Rodríguez, A. Luna, I. Candela, R. Mujal, R. Teodorescu, and F. Blaabjerg, "Multiresonant frequency-locked loop for grid synchronization of power converters under distorted grid conditions," *IEEE Trans. Ind. Electron.*, vol. 58, no. 1, pp. 127–138, Jan. 2011.

[30] *IEEE Standard Definitions for the Measurement of Electric Power Quantities Under Sinusoidal, Nonsinusoidal, Balanced, or Unbalanced Conditions*, IEEE Standard 1459-2010 (Revision IEEE Std 1459-2000), 2010.

[31] W. Yao, M. Chen, J. Matas, J. M. Guerrero, and Z.-M. Qian, "Design and analysis of the droop control method for parallel inverters considering the impact of the complex impedance on the power sharing," *IEEE Trans. Ind. Electron.*, vol. 58, no. 2, pp. 576–588, Feb. 2011.

[32] *IEEE Recommended Practices and Requirements for Harmonic Control in Electrical Power Systems*, IEEE Standard 519-1992, 1993.

[33] S. Sahoo and S. Mishra, "A distributed finite-time secondary average voltage regulation and current sharing controller for DC microgrids," *IEEE Trans. Smart Grid*, vol. 10, no. 1, pp. 282–292, Jan. 2019.

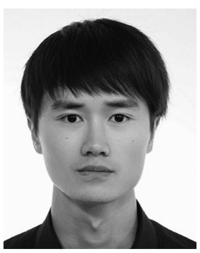

Junjie Xiao (Graduate Student Member, IEEE) received the B.Sc. degree in electrical engineering from Sichuan Agricultural University, Yaan, China, in 2018, and the M.Sc. degree from Xi'an Jiaotong University, Xi'an, China, in 2021. He is currently pursuing the Ph.D. degree in electrical engineering with the Delft University of Technology, Delft, The Netherlands.

His research interests include the cyber security of microgrids and coordinated control of grid-tied inverters.

Lu Wang (Graduate Student Member, IEEE) received the B.Sc. degree in electrical engineering from the Beijing Institute of Technology, Beijing, China, in 2015, and the M.Sc. degree (cum laude) in electrical power engineering from the Delft University of Technology, Delft, The Netherlands, in 2018, where he is currently pursuing the Ph.D. degree with the DC Systems, Energy Conversion and Storage Group on Power Quality of EV Charing.

Pavol Bauer (Senior Member, IEEE) received the master's degree in electrical engineering from the Technical University of Kosice in 1985, the Ph.D. degree from the Delft University of Technology in 1995, and the Doctoral degree (Hons.) from Politehnica University Timisioira, Romania. He is a Professor with the Brno University of Technology, Czech Republic, in 2008, and the Delft University of Technology in 2016. He is currently a Full Professor with the Department of Electrical Sustainable Energy, Delft University of Technology, and the Head of DC Systems, Energy Conversion and Storage Group. He is also a Honorary Professor with Politehnica University Timisioira. From 2002 to 2003, he was working partially at KEMA (DNV GL, Arnhem) on different projects related to power electronics applications in power systems. He published over 180 journal and 450 conference papers in his field (with H factor Google scholar 58 and Web of Science 41). He is an author or coauthor of eight books, holds ten international patents, and organized several tutorials at the international conferences. He has worked on many projects for industry concerning wind and wave energy, power electronic applications for power systems such as Smarttrafo; HVDC systems, projects for smart cities, such as PV charging of electric vehicles, PV and storage integration, contactless charging; and he participated in several Leonardo da Vinci, H2020 and Electric Mobility Europe EU projects as a project partner (ELINA, INETELE, E-Pragmatic, Micact, Trolly 2.0, OSCD, P2P, Progressus, Tulip, and Flow), and a coordinator (PEMCWebLab.com-Edipe, SustEner, and Eranet DCMICRO). His main research interest is power electronics for charging of electric vehicles and dc grids. He is a Former Chairman of Benelux IEEE Joint Industry Applications Society, Power Electronics and Power Engineering Society chapter, the Chairman of the Power Electronics and Motion Control Council and Benelux IEEE Industrial Electronics chapter, and a member of the Executive Committee of European Power Electronics Association and International Steering Committee at numerous conferences.

Zian Qin (Senior Member, IEEE) received the B.Eng. degree in electrical engineering from Beihang University, Beijing, China, in 2009, the M.Eng. degree in electrical engineering from the Beijing Institute of Technology, Beijing, in 2012, and the Ph.D. degree in electrical engineering from Aalborg University, Aalborg, Denmark, in 2015.

He is an Assistant Professor with the Delft University of Technology, Delft, The Netherlands. In 2014, he was a Visiting Scientist with Aachen University, Aachen, Germany. He has published more than 100 journals/conference papers, four book chapters, two international patents, and also worked on several European and Dutch national projects in these areas. His research interests include power quality and stability of power electronics-based grid, and solid state transformers. He is an Associate Editor of IEEE TRANSACTIONS ON INDUSTRIAL ELECTRONICS, and a Guest Associate Editor of IEEE JOURNAL OF EMERGING AND SELECTED TOPICS and IEEE TRANSACTIONS ON ENERGY CONVERSION. He is a Distinguished Reviewer for 2020 of IEEE TRANSACTIONS OF INDUSTRIAL ELECTRONICS. He served as the Technical Program Chair of IEEE-PEDG 2023, IEEE-ISIE 2020, and IEEE-COMPEL 2020.